Slow Strain Rate Tensile Tests of Irradiated Austenitic Stainless Steels in Simulated PWR Environment

Y. Chen[1], B. Alexandreanu[1], W. K. Soppet[1], W. J. Shack[1], K. Natesan[1], and A. S. Rao[2]

[1] Nuclear Engineering Division, Argonne National Laboratory;
9700 South Cass Ave., Argonne, IL 60439, USA
[2] US Nuclear Regulatory Commission; Washington, DC 20555, USA

Keywords: IASCC, stainless steels, PWR, slow strain rate tensile

Abstract

Irradiation-assisted stress corrosion cracking is of concern for the safe and economic operation of light water reactors. In this study, cracking susceptibility of austenitic stainless steels was investigated by using slow strain rate tensile (SSRT) tests in a simulated pressurized water reactor (PWR) environment. The specimens were irradiated to 5, 10, and 48 dpa in the BOR60 reactor at 320°C. The SSRT results showed that yield strength was increased significantly in irradiated specimens while ductility and strain hardening capability were decreased. Irradiation hardening was found to be saturated below 10 dpa. The irradiated yield strength of cold-worked specimens was higher than that of solution-annealed specimens. Fractographic examinations were also performed on the tested specimens, and the dominant fracture morphology was ductile dimples. Intergranular cracking was rarely seen on the fracture surface. Transgranular cleavage cracking, however, was found more frequently on the specimen tested in simulated PWR environment.

1. Introduction

Irradiation-assisted stress corrosion cracking (IASCC) is a key issue concerning aging light water reactors. Nonsensitized austenitic stainless steels (SSs) used in reactor core internals can experience premature failures after extended neutron exposure. Cracking has occurred in SS components such as fuel cladding, absorber tubes, core shrouds, and top guides in boiling water reactors (BWRs), and fuel cladding, control rod cladding, and baffle former bolts in pressurized water reactors (PWRs) [1-4]. The elevated cracking susceptibility has been attributed to both irradiation damage in austenitic SSs and the aggressive environment of reactor coolants. For BWRs, a fast neutron fluence of 3~5 x 10^{20} n/cm^2 (E>1MeV), or 0.45~0.75 displacements per atom (dpa), has been found to be necessary for the occurrence of IASCC [5,6]. This cracking behavior is closely related to the oxidation rate of SSs, and thus, is sensitive to corrosion potential [7,8]. In PWRs, environmentally-enhanced cracking occurs at a higher neutron fluence, and IASCC can only be seen above 1~2 x 10^{21} n/cm^2 (E>1MeV) or 1.5~3 dpa [6]. Nonetheless, even in a low-potential environment such as in a hydrogenated primary coolant, austenitic SSs are not immune to IASCC. Irradiation damage plays an important role in elevating cracking susceptibility under this condition.

Neutron irradiation has a profound impact on microstructural and microchemical changes in austenitic SSs [9-11]. Displacement damage resulting from fast neutron bombardments gives rise to defects and defect clusters in matrixes and alters local alloy chemistry, leading to second-phase precipitates and segregations at grainboundaries. There is no doubt that irradiation-

induced microstructural and microchemical changes are the root cause of the elevated cracking susceptibility. A number of micro-mechanisms associated with irradiation damage have been considered for IASCC [12,13]. While significant progress has been made to understand cracking response to corrosion potential, the exact mechanism operating under the PWR environment remains unclear [7,8]. At present, the data for PWR core internals are still limited, and the key metallurgical variables have not been identified. Whether or not irradiation embrittlement alone is sufficient to explain the intergranular cracking in PWR core internals needs to be further investigated. A better understanding of cracking mechanism in the PWR environment is crucial not only for establishing possible countermeasures to mitigate IASCC, but also for developing predictive and regulatory methodology.

In this study, slow strain rate tensile (SSRT) tests were performed in simulated PWR water at 315°C on several austenitic SSs irradiated in the BOR-60 reactor. The fracture surfaces of the tested SSRT specimens were examined by a shielded scanning electron microscopy (SEM). The effects of thermomechanical treatments and irradiation dose on SSRT behavior were discussed.

2. Experimental

2.1 Materials and Specimens

Materials included in this study are 300 series SSs in both solution-annealed (SA) and 35% cold-worked (CW) conditions. Table 1 shows the compositions of these alloys. For 304 grade SSs, there are one normal 304 SS (A5), two low-carbon SSs (A10 and A11), and two high-purity low-carbon SSs with different oxygen contents (A8 and A9). For 316 grade SSs, there are two low-carbon, high-nitrogen SSs with and without Ti addition (B3 and B4), and two normal 316 SSs (B5 and B6).

Flat tensile specimens about 1-inch long were used for the SSRT tests. Figure 1 shows the dimensions of the tensile specimen.

Table 1. Materials included in this study (wt.%).

Mat. Type	Material*	Mat. Code	Composition (wt.%)								
			Ni	Si	P	S	Mn	C	N	Cr	Other Elements
304, 304L	304 CW	A5	8.23	0.47	0.018	0.002	1.00	0.060	0.070	18.43	B <0.001
	304L SA / CW	A10 / A11	8.91	0.46	0.019	0.004	1.81	0.016	0.083	18.55	B< 0.001
	HP 304L SA, high O	A8	9.03	0.03	<0.005	0.005	1.11	0.005	0.003	19.21	O 0.047, Mo <0.005
	HP 304L SA, low O	A9	9.54	0.01	0.001	0.002	1.12	0.006	<0.001	19.71	O 0.008, Mo 0.02
316, 316L	316 LN SA	B3	12.20	0.70	0.007	0.002	0.97	0.019	0.103	17.23	Mo 2.38, Cu 0.21
	316 LN-Ti SA	B4	12.30	0.72	0.007	0.002	0.92	0.012	0.064	17.25	Mo 2.38, Ti 0.027, Cu 0.21
	316 SA and CW	B5 / B6	10.24	0.51	0.034	0.001	1.19	0.060	0.020	16.28	Mo 2.08, B<0.001

* SA = solution annealed, CW = cold worked, HP = high purity.

2.2 Irradiations

All specimens were irradiated in BOR-60, a sodium-cooled fast breeder reactor located in the Research Institute of Atomic Reactors (RIAR), Dimitrovgrad, Russia. Irradiations were performed in two experiments, Boris-6 and -7, and at three displacement dose levels (5, 10, and 48 dpa) [14]. Neutron dosimeters were loaded in the irradiation rig along with the specimens, and the final dosimetry was carried out by RIAR after irradiation. During the irradiation experiments, the tensile specimens were separated in bundles (four specimens in each bundle) and were in contact with sodium coolant. The irradiation temperature was controlled by

monitoring the inlet and outlet sodium temperatures, which were kept at 315 and 325°C, respectively. Magnesium-zinc eutectic thermal monitors were also placed among the specimen bundles to verify the irradiation temperature.

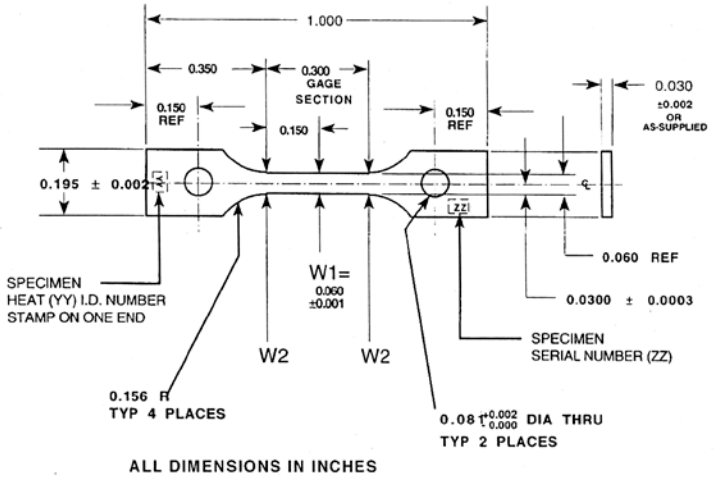

Figure 1. Slow strain rate tensile specimen used in this study.

2.3 Slow Strain Rate Tensile Test

The SSRT tests were conducted in the Irradiated Materials Laboratory at Argonne. This facility is equipped with a worm gear actuator, a set of gear reducers, and a variable speed motor with control. A simulated PWR water environment was provided by a recirculation loop, which includes a storage tank, a high-pressure pump, a back pressure regulator, and a test autoclave. The system is also equipped with online conductivity and pH sensors and an electrochemical potential (ECP) cell to monitor the test condition.

Table 2 summarizes the SSRT tests performed in this study. All tests were conducted at 315°C and 1800 psig under a constant strain of 7.4×10^{-7} s^{-1}. The simulated PWR water contained approximately 2 ppm Li, 1000 ppm B, 2 ppm dissolved hydrogen, and <10 ppb dissolved oxygen. The conductivity of the water was about 20 μS/cm, and its pH was 6.6 at room temperature. The flow rate of the system was maintained at 15-30 ml/min during the tests. Prior to each test, the specimen was exposed to the simulated PWR water for 24 to 30 hours to stabilize environmental conditions. After the tests, fracture surfaces of the tested samples were examined with a shielded scanning electron microscope (SEM).

Table 2. Slow strain rate tensile tests performed in this study.

Material Type	Material	Material Code	Dose (dpa)		
			5	10	48
304, 304L	304 CW	A5	-	-	√
	304L SA	A10	-	√	-
	304L CW	A11	-	√	√
	304-like alloy	A12	-	√	√
	HP 304L SA, High O	A8	-	√	√
	HP 304L SA, Low O	A9	-	√	√
316, 316L	316LN SA	B3	√	√	-
	316LN-Ti SA	B4	-	-	√
	316 SA	B5	-	-	√
	316 CW	B6	√	√	√

3. Results and Discussion

3.1 Type 304 and 304L SSs

A 48-dpa CW Type 304 SS specimen was tested in PWR water, and the stress-strain curve is shown in Fig. 2. Very little work hardening remained in this sample after irradiation, and the total elongation was just 3.6%. Figure 3 shows the fracture surface of the tested sample. While dimples are the dominant features of the fracture surface at this dose, small transgranular areas appear both on the surface and at the interior of the sample (Fig. 3). No intergranular cracking can be seen in this sample. Overall, visible brittle areas are less than 2% of the whole fracture surface.

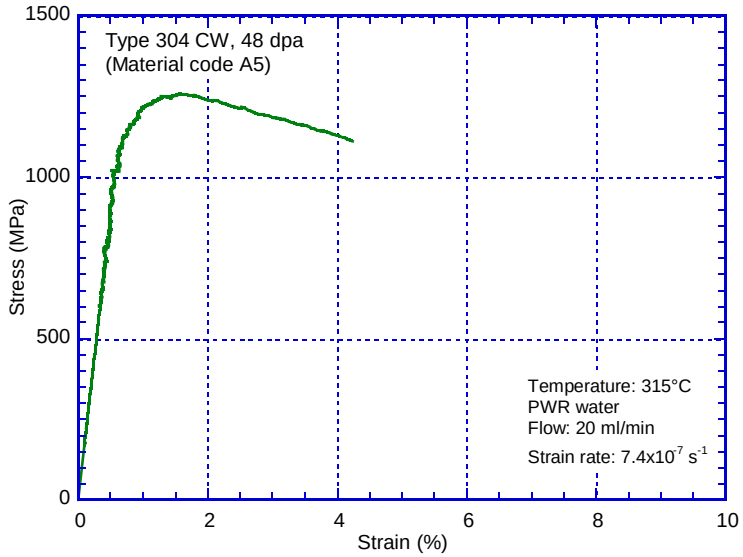

Figure 2. SSRT stress-strain curve of a CW Type 304 SS irradiated to 48 dpa.

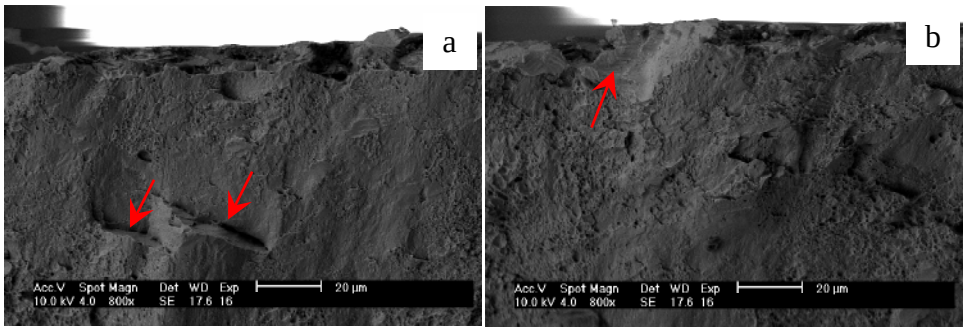

Figure 3. Transgranular cracking in 48-dpa CW 304 SS at sample interior (a) and on surface (b).

Figure 4 shows stress-strain curves for three Type 304L SS specimens: two 10-dpa samples of SA and CW specimens and one 48-dpa CW specimen. The SA and CW samples exhibit very different stress-strain curves. Regardless of their dose levels, the CW samples show much higher yield stresses and less elongation. The SSRT behaviors of the two CW samples are similar, with a slightly higher yield stress and less elongation for the 48-dpa sample. Ductile dimples are the main morphology of all three fracture surfaces, but detailed observations reveal several brittle areas in the CW samples as shown in Fig. 5. The 10-dpa SA sample shows a fully ductile failure, and its entire fracture surface is covered with large dimples (Fig. 5a). For the 10-dpa CW sample, although most of fracture surface exhibits a ductile dimple morphology, small

transgranular cracking areas are evident, as shown in Fig. 5b. In the 48-dpa CW sample, areas of cleavage and mixed mode cracking are observed among ductile dimples that cover the majority of the fracture surface (Figs. 5c-d). Although the dominant failure mode is dimple fracture for all 304L samples, brittle morphology is more likely in CW alloys and at higher doses.

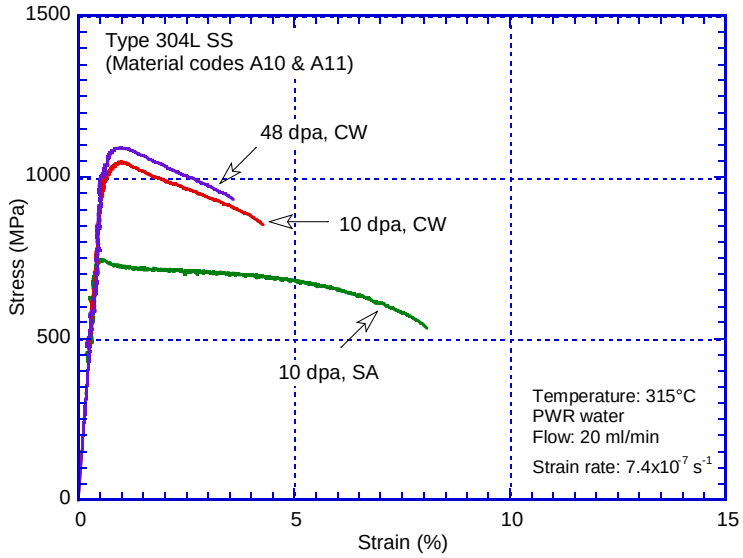

Figure 4. SSRT stress-strain curves of SA and CW Type 304L SSs irradiated to 10 and 48 dpa.

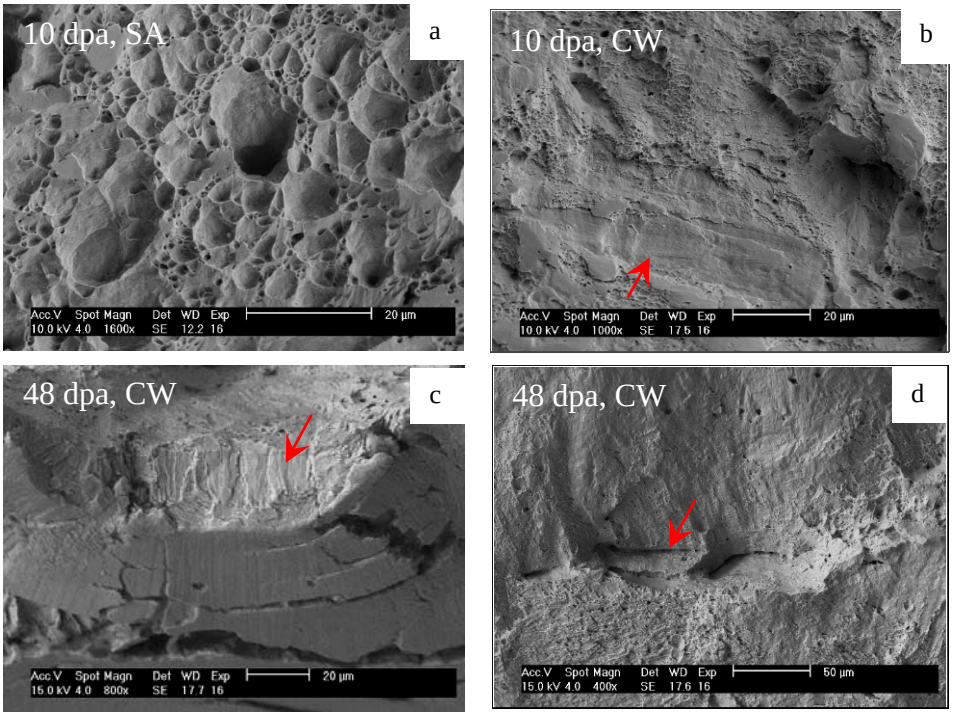

Figure 5. Fracture morphology of 304L SSs: (a) large dimples in 10-dpa SA sample, (b) transgranular areas in 10-dpa CW sample, and (c, d) cleavage and mixed mode fracture in 48-dpa CW sample.

The SSRT test results for HP 304L SSs with low (~0.008 wt.%) and high oxygen (~0.047 wt.%) contents are shown in Fig. 6. For these two alloys, the stress-strain curves for all doses display a dramatic load drop beyond yield. The same behavior was also observed in previous SSRT tests

in a simulated BWR environment [5]. No strain hardening was observed for either alloy at both doses. Total elongations are also similar except for the 48-dpa high-O sample, whose initial thickness was considerably less than that of the other samples due to a machining issue. The fracture surfaces are shown in Fig. 7. Significant necking is observed for the two low-O samples, indicating good ductility of this alloy. At both 10 and 48 dpa, the reduction of area (RA) for the low-O specimens is about 80%, in contrast to 60% for high-O specimens. Despite the difference in RA, detailed observations of the fracture surfaces reveal little difference between the two alloys, as shown in Fig. 8. Both low- and high-oxygen HP 304L SSs display dimple fracture regardless of their doses.

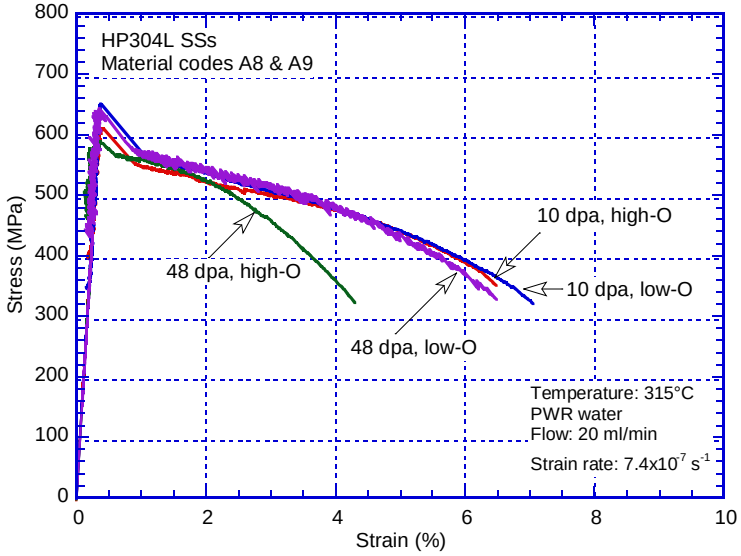

Figure 6. SSRT stress-strain curves of HP 304L SSs with low and high oxygen contents irradiated to 10 and 48 dpa.

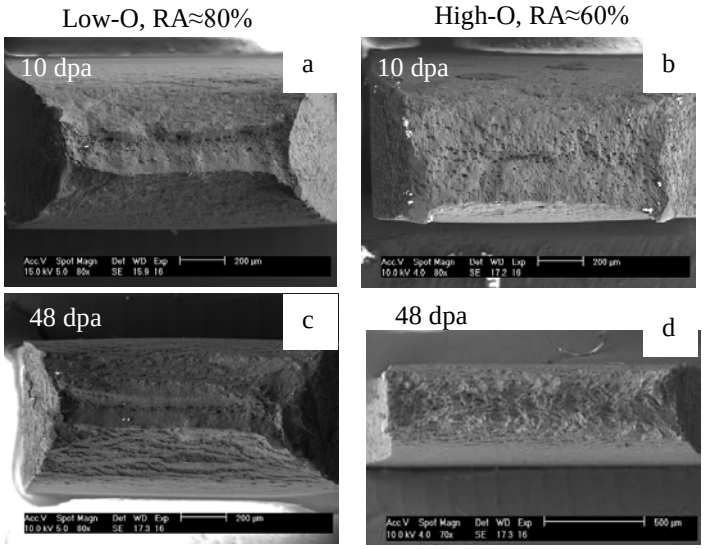

Figure 7. Fracture surfaces of HP 304L SSs: (a) low-O and (b) high-O content at 10 dpa, and (c) low-O and (d) high-O content at 48 dpa.

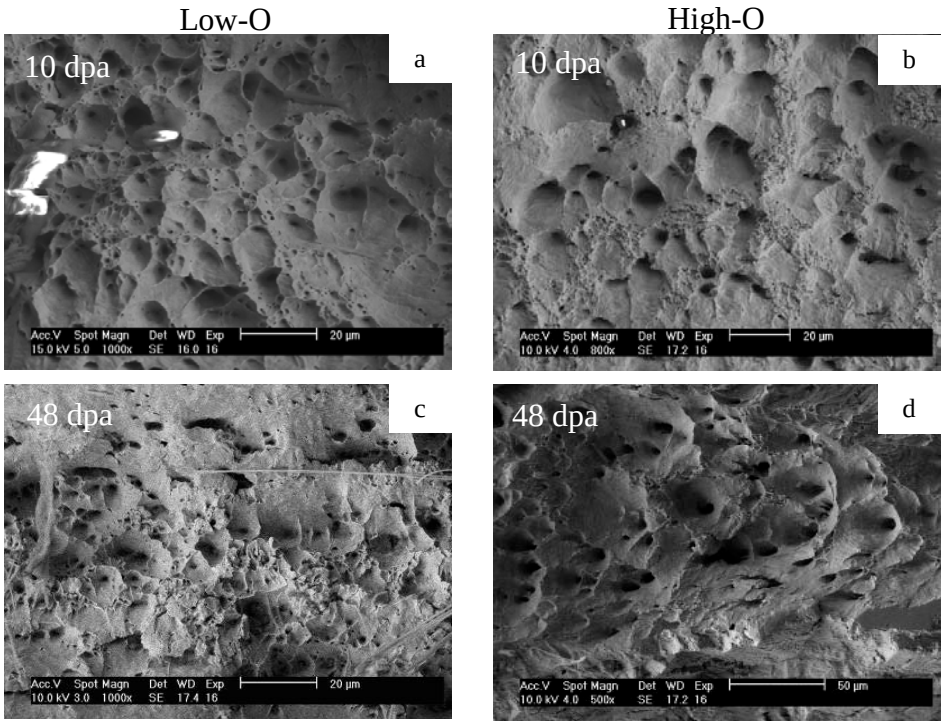

Figure 8. Similar dimple fracture for HP304L SSs: (a) low-O and (b) high-O content at 10 dpa, and (c) low-O and (d) high-O content at 48 dpa.

3.2 Types 316 and 316L SSs

Three CW and one SA Type 316 SS specimens were tested in simulated PWR water. As shown in Fig. 9, the yield stress of the SA sample is significantly lower than that of the CW samples. At the same dose (48 dpa), total elongation is also much larger in the SA than the CW materials. It appears that a significant effect of thermomechanical treatment on plastic deformation remains after irradiation up to 48 dpa. For the CW specimens, the yield strengths are similar at all three doses, indicating saturation behavior with the irradiation hardening.

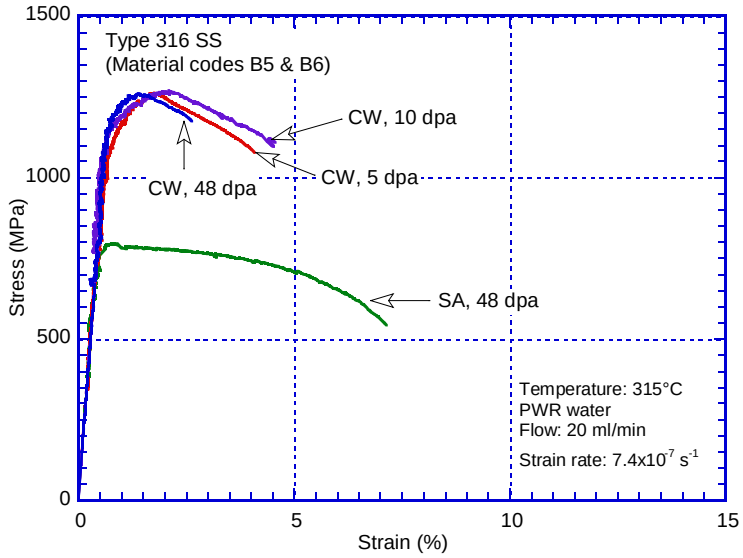

Figure 9. SSRT stress-strain curves of SA and CW Type 316 SSs irradiated to 5, 10, and 48 dpa

The dominant fracture morphology is dimples for all Type 316 SS specimens tested in simulated PWR water. Small brittle areas are evident in the SA and CW samples. In the 48-dpa SA sample, cleavage and mixed mode fracture can be seen (Fig. 10a-b). Some intergranular features are also visible. By contrast, no intergranular cracking can be seen in all CW samples, and areas of mixed mode fracture are apparent (Fig. 10c-d). Despite a much lower elongation of the CW sample in the SSRT tests at 48 dpa, its fracture surface does not appear more susceptible to cracking than that of the SA sample at the same dose.

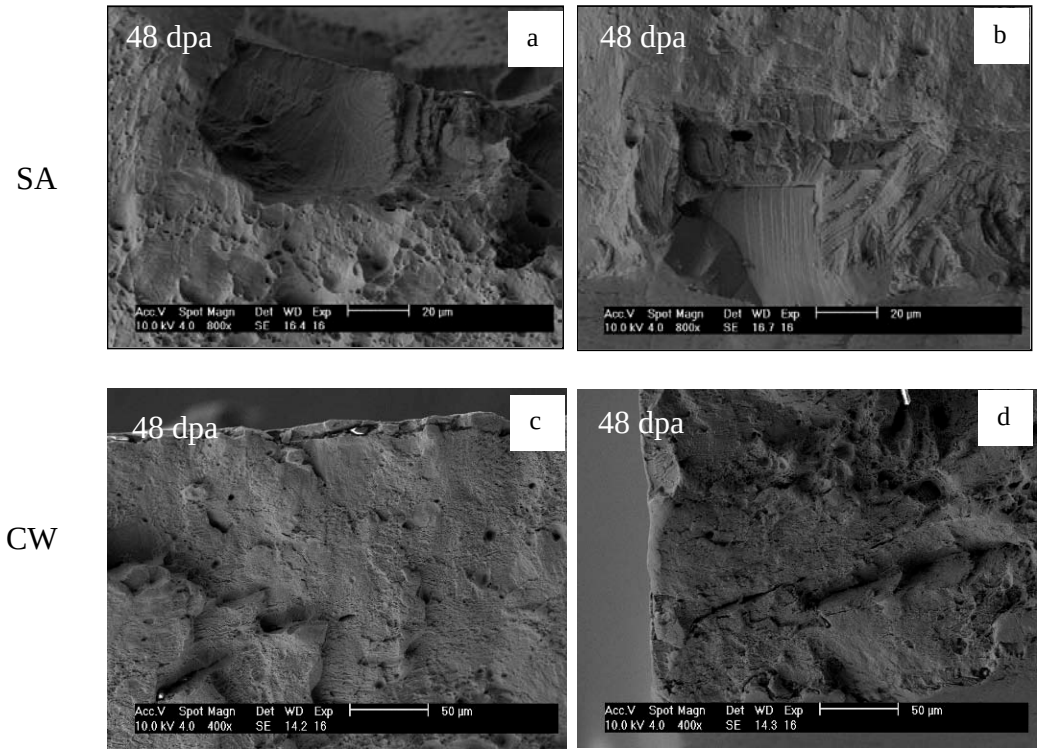

Figure 10. Fracture surfaces of 48-dpa Type 316 SSs: cleavage (a) and mixed mode cracking (b) in the SA specimen, and mixed mode cracking in the CW specimen (c, d).

Two low-carbon, high-nitrogen 316 SSs with and without Ti addition are also included in this study. For the alloy without Ti, the yield strength increases and elongation decreases with dose from 5 to 10 dpa (Fig. 11). The specimen with Ti addition received a dose of 48 dpa, and its yield stress and total elongation are comparable to that of the10-dpa specimen without Ti. For the three 316LN SS specimens, the fracture surfaces appeared to be similar. A closer look at the fracture surfaces revealed fine dimple morphology for all samples, as shown in Fig. 12. The specimen with Ti addition has slightly larger dimples. Small areas of mixed mode fracture are present in all samples. The Ti addition does not appear to change the cracking behavior of 316LN SS.

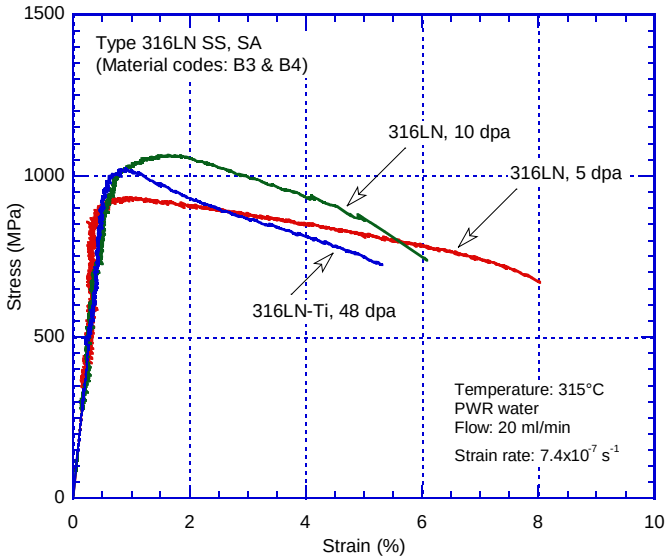

Figure 11. SSRT stress-strain curves of Type 316LN with and without Ti addition irradiated to 5, 10 and 48 dpa.

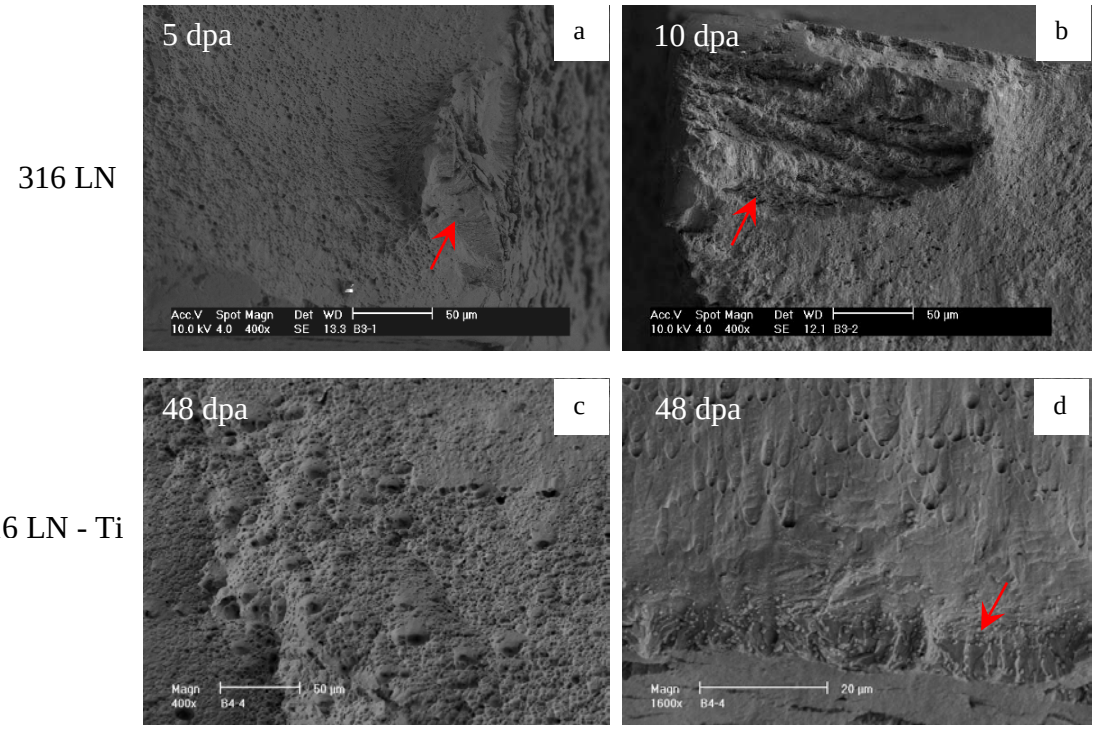

Figure 12. Fracture surfaces of 316LN SSs: (a) 5-dpa sample, (b) 10-dpa sample, and (c, d) 316LN-Ti sample at 48 dpa.

3.3 Dose Effects

Irradiation hardening and embrittlement have a significant impact on SSRT behavior. To assess cracking susceptibility of austenitic SSs, dose dependences of irradiation hardening and embrittlement are needed for temperatures and doses relevant to light water reactors. To reveal the effects of irradiation dose, all SSRT results in this study are plotted in Fig. 13 along with

other BOR-60 and Halden results obtained at≈290°C . As shown in Fig. 13a, all data fall into two scatter bands that represent two thermomechanical conditions, SA and CW. In general, the irradiated yield stress is higher for CW than for SA materials. The yield stress increases rapidly in the low dose region up to 5 dpa and eventually saturates at 5-10 dpa. Between 10 and 48 dpa, the yield stress is nearly unchanged. Since a wide range of austenitic SSs is included in these results, heat-to-heat variation is probably responsible for the apparent large scatter in the results. The difference in yield strength between SA and CW materials is better revealed with a single alloy. As shown in Fig. 13b, the higher yield stress generated from CW is not affected by the BOR-60 irradiation, and the differences between SA and CW materials remain the same up to 48 dpa.

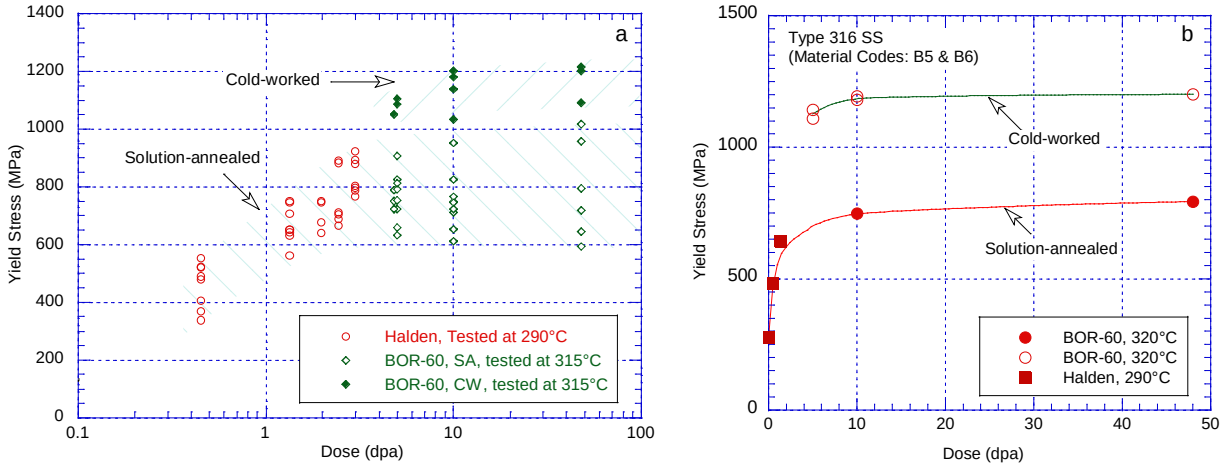

Figure 13. SSRT yield strength as a function of irradiation dose: (a) all materials tested on the BOR-60 and Halden specimens, and (b) a single material, Type 316 SS.

Figure 14 shows the total elongations as a function of dose. It should be noted that elongations of Halden and BOR-60 specimens are not directly comparable because of their different gauge dimensions [5,15]. Thus, the dose dependence of total elongation in Fig. 14 may not be quantitatively accurate. Nonetheless, a decreasing trend of ductility is indicated with increasing dose. The total elongations are also different for the CW and SA materials. The effect of thermomechanical treatment is illustrated by the two lines constructed to fit the Type 316 SS data.

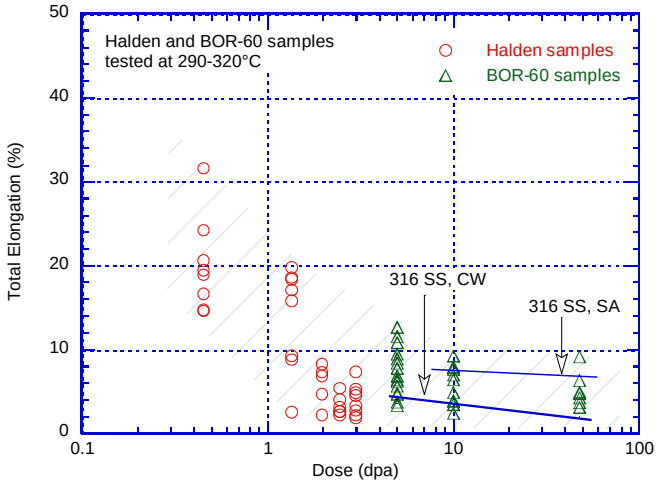

Figure 14. Total elongation as a function of irradiation dose for BOR-60 and Halden specimens.

4. Summary

Slow-strain rate tensile tests have been performed in simulated PWR water at 315°C on selected 304 and 316 grades of stainless steels. The specimens were irradiated in the BOR-60 reactor to 5, 10, and 48 dpa. Significant irradiation hardening was observed in all SSRT tests. The saturation of irradiation hardening appears to be below 10 dpa. Work hardening capability decreaseed considerably in the irradiation specimens, and above 5 dpa, very little work hardening was evident. The SSRT behavior of SA specimens was compared with that of the CW specimens under similar irradiation and test conditions. The effect of thermomechanical treatment on SSRT behavior remained unchanged up to 48 dpa.

Ductile dimple fracture was the dominant morphology for all SSRT tests in the PWR water environment. Intergranular cracking was only seen in the SA Type 316 SS irradiated to 48 dpa. Cleavage cracking was found in some samples at the fracture surface, and transgranular or mixed mode cracking was also seen in high-dose samples. The overall fraction of brittle fracture was low (a few percent), even at 48 dpa. Despite the difference in total elongations, post-irradiation cracking susceptibility evaluated from the fracture surfaces appeared similar between SA and CW samples tested in simulated PWR water.

Acknowledgments

The authors would like to thank Dr. O. K. Chopra for his invaluable contribution to this program. Dr. Raj Pathania and Dr. Peter Scott are acknowledged for arranging irradiations through the Cooperative IASCC Research (CIR) program. The authors would also like to thank Dr. Regis P. Shogan and Mr. Anders Jenssen for transferring the irradiated specimens from Russia. We are also grateful to W. H. Cullen, Jr., R. Tregoning, and S. Crane for many helpful discussions and suggestions. This work is sponsored by the Office of Nuclear Regulatory Research, U.S. Nuclear Regulatory Commission, under Job Code N6519; Program Manager: A. S. Rao.

References

1. Craig F. Cheng, “Intergranular Stress-Assisted Corrosion Cracking of Austenitic Alloys in Water-Cooled Nuclear Reactors,” J. Nucl. Mater., **56** (1975) 11-33.

2. F. Garzarolli, H. Rubel, and E. Steinberg, “Behavior of Water Reactor Core Materials with Respect to Corrosion Attack,” Proc. Intl. Symp. on Environmental Degradation of Materials in Nuclear Power Systems -- Water Reactors, NACE, Houston, TX, pp. 1-24, 1984.

3. F. Garzarolli, D. Alter, and P. Dewes, “Deformability of Austenitic Stainless Steels and Nickel-Base Alloys in the Core of a Boiling and a Pressurized Water Reactor,” Proc. Intl. Symp. on Environmental Degradation of Materials in Nuclear Power Systems - Water Reactors, American Nuclear Society, La Grange Park, IL, pp. 131-138, 1986.

4. R. L. Jones, J. D. Gilman, and J. L. Nelson, “Controlling Stress Corrosion Cracking in Boiling Water Reactors,” J. Nucl. Mater., **143** (1993) 111.

5. Y. Chen, O. K. Chopra, W. K. Soppet, N. L. Dietz Rago, and W. J. Shack, “IASCC Susceptibility of Austenitic Stainless Steels and Alloy 690 in High Dissolved Oxygen Water

Environment," Proc. 13th Intl. Symp. on Environmental Degradation of Materials in Nuclear Power Systems - Water Reactors, 2007.

6. P. Scott, "A Review of Irradiation Assisted Stress Corrosion Cracking", J. Nucl. Mater., **211**, (1994) 101-122.

7. P. L. Andresen, F. P. Ford, S. M. Murphy, and J. M. Perks, "State of Knowledge of Radiation Effects on Environmental Cracking in Light Water Reactor Core Materials," Proc. 4th Intl. Symp. on Environmental Degradation of Materials in Nuclear Power Systems--Water Reactors, NACE, Houston, TX, pp. 1.83-1.121, 1990.

8. G. S. Was, and P. L. Andresen, "Stress Corrosion Cracking Behavior of Alloys in Aggressive Nuclear Reactor Core Environments," Corrosion, **63** (1), (2007), 19.

9. J. O. Stiegler and L. K. Mansur, "Radiation Effects in Structural Materials," Ann. Rev. Mater. Sci., **9** (1979) 405.

10. S. J. Zinkle, P. J. Maziasz, and R. E. Stoller, "Dose Dependence of the Microstructural Evolution in Neutron-Irradiated Austenitic Stainless Steel," J. Nucl. Mater., **206** (1993) 266.

11. P. J. Maziasz, "Overview of Microstructural Evolution in Neutron-Irradiated Austenitic Stainless Steels," J. Nucl. Mater., **205** (1993) 118.

12. G. S. Was, and S. M. Bruemmer, "Effect of Irradiation on Intergranular Stress Corrosion Cracking," J. Nucl. Mater., **216** (1994) 326.

13. S. M. Bruemmer, and G. S. Was, "Microstructural and Microchemical Mechanisms Controlling Intergranular stress corrosion cracking in light-water-reactor systems," J. Nucl. Mater., **216** (1994) 348.

14. Electric Power Research Institute, "CIR II Program: Description of the Boris 6 and 7 Experiment in the BOR-60 Fast Breeder Reactor," Report No. 1011787, Palo Alto, CA, 2005.

15. Y. Chen, O. K. Chopra, W. K. Soppet, W. J. Shack, Y. Yang, and T. Allen, "Cracking Behavior and Microstructure of Austenitic Stainless Steels and Alloy 690 Irradiated in BOR-60 Reactor, Phase I," Report ANL/09-32, Argonne National Laboratory, 2010.